Computer Methods in Biomechanics and Biomedical Engineering
Vol. 14, No. 5, May 2011, 459–468

Taylor & Francis
Taylor & Francis Group

Simulations of the contractile cycle in cell migration using a bio-chemical–mechanical model

Sangyoon J. Han[a] and Nathan J. Sniadecki[a,b]*

[a]*Department of Mechanical Engineering, University of Washington, Seattle, WA, USA;* [b]*Department of Bioengineering, University of Washington, Seattle, WA, USA*

(*Received 1 October 2010; final version received 11 January 2011*)

Cell migration relies on traction forces in order to propel a cell. Several computational models have been developed that help explain the trajectory that cells take during migration, but little attention has been placed on traction forces during this process. Here, we investigated the spatiotemporal dynamics of cell migration by using a bio-chemical–mechanical contractility model that incorporates the first steps of cell migration on an array of posts. In the model, formation of a new adhesion causes a reactivation of stress fibre assembly within a cell. The model was able to predict the spatial distribution of traction forces observed with previous experiments. Moreover, the model found that the strain energy exerted by the traction forces of a migrating cell underwent a cyclic relationship that rose with the formation of a new adhesion and fell with the release of an adhesion at its rear.

Keywords: cell migration; contractility; computational modelling of cell mechanics; stress fibres

1. Introduction

Cell migration plays an essential role in wound healing, vascular remodelling, immune response and cancer metastasis (Bray 2001; Chicurel 2002). To better understand how each of these biological events occurs, a wide range of mathematical and computational models were developed (Tranquillo et al. 1988; Chaplain 2000; Gerisch and Chaplain 2008; Thackham et al. 2009). Cell migration in these models was commonly simulated using a partial differential equation based on diffusion physics, because importance was placed on the number of cells that were guided to a spatial point chemotactically. On the cellular level, however, migration involves the integration of dynamic changes in focal adhesions, cytoskeletal structures, and chemical and mechanical signals from the extracellular matrix. These changes are incorporated into a cyclic progress where a cell extends its leading edge, forms new adhesions at the front, contracts its cytoskeleton and releases adhesions at the rear (Lauffenburger and Horwitz 1996; Sheetz et al. 1999).

Although mechanical and/or chemical gradients in the environment can affect the direction that a cell migrates (Carter 1967; Devreotes and Zigmond 1988; Lo et al. 2000; Li et al. 2002; Giannone and Sheetz 2006), it is the traction forces that actually drive the migration. Myosin-based traction forces are transmitted to a substrate via focal adhesions to pull a cell in the direction of its polarised leading edge. The adhesions at the rear need to detach in order to allow a cell to move forward. Although adhesion release depends on interactions among actin, actin-binding proteins, signalling molecules and enzymes (Kirfel et al. 2004; Rigort et al. 2004), traction forces may also contribute to the release by breaking adhesive bonds at the rear (Lauffenburger and Horwitz 1996; Sheetz et al. 1999). Whole cell models were developed which incorporate the signalling and mechanics in actin polymerisation, myosin contraction and adhesion dynamics (DiMilla et al. 1991; Gracheva and Othmer 2004; Maree et al. 2006; Dokukina and Gracheva 2010). These models have provided significant insights into trajectory of cells during directed cell migration, e.g. chemotaxis, haptotaxis and durotaxis. However, modelling of cell migration would be more accurate if it could describe the traction forces that cells generate in addition to locomotion.

Several kinds of assays have recently been developed to measure and characterise traction forces of cells (Harris et al. 1980; Galbraith and Sheetz 1997; Dembo and Wang 1999; Munevar et al. 2001; Tan et al. 2003; Mitrossilis et al. 2009). In particular, arrays of microfabricated posts were used to study single cell contractility (Tan et al. 2003; Saez et al. 2005; Ghibaudo et al. 2008), cell-cell adhesion strength (Liu et al. 2010), platelet contractile forces (Liang et al. 2010) and traction forces during the migration of cell monolayers (du Roure et al. 2005). Even though the topology of the post arrays is not continuous, cells are not restricted from spreading and migrating (du Roure et al. 2005; Lemmon et al. 2005). A typical traction force vector map of a single cell is demonstrated in Figure 1. It is generally noted that a cell exerts traction forces in the centripetal direction due to the arrangement of stress fibres, which are bundles of actin filaments cross-linked with myosin and α-actinin.

*Corresponding author. Email: nsniadec@uw.edu

ISSN 1025-5842 print/ISSN 1476-8259 online

DOI: 10.1080/10255842.2011.554412
http://www.informaworld.com

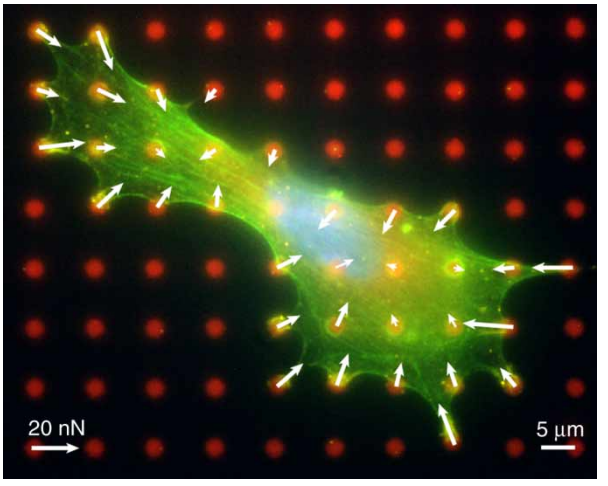

Figure 1. Human pulmonary artery endothelial cell on an array of posts (green: actin, red: post, blue: nucleus). Vectors denote the traction forces produced by the cell's deflection of the posts.

The post arrays have yielded many interesting findings about a cell's contractile response to mechanical changes in the substrate, and in turn, these findings have helped to generate new ideas in modelling cell mechanics. In particular, a bio-chemical–mechanical model was developed and used to explain the findings from post array studies (Deshpande et al. 2006, 2007; McGarry et al. 2009). The model consists of an activation signal that elicits actin polymerisation and myosin light chain phosphorylation, the degree of assembly of actin and myosin into a stress fibre and a force–velocity relationship between contraction rate and cytoskeletal tension that is akin to Hill's muscle model.

Our goal in this paper is to evaluate the appropriateness of the bio-chemical–mechanical model in quantitatively predicting the migration of cells on arrays of posts in both one- and two-dimensions. The model takes into account a fundamental feature of cell migration: traction force generation. In addition, the role that adhesion dynamics has in regulating cytoskeletal tension was added to the model. These properties are expressed during three main steps in cell migration: initial contraction up to a steady state, a second activation of contractility after new adhesion formation and release of adhesion at the trailing edge of the cell. This model predicts key spatial and temporal features of cellular contractility during migration, which includes large traction force at the leading and trailing edges, movement of the force equilibrium point during the steps of migration and a contractility drop during the release phase. Some of the results match with findings from experimental studies, whereas others provide new insights for consideration.

2. Mathematical model

This section discusses the modelling of contractility-based migration model with each component in the contractility model, its biological relevance and assumptions being discussed. The computational methods that incorporate the contractility model into cell migration are described for 1D and 2D simulations.

2.1 Contractility model

The contractility model used in this study is based on the bio-chemical–mechanical model previously developed (Deshpande et al. 2007). For the purpose of our study, however, the model was adapted to suit cell migration mechanics by adding a few more assumptions, which are to be discussed in the following section. Briefly, the contractility model consists of three components: a time-decaying activation signal, actin–myosin assembly level and a linearised version of the force–velocity equation for actin–myosin force production.

2.1.1 Activation signal

An activation signal C that subsequently triggers actin polymerisation and myosin phosphorylation starts the contractile activity within a cell. This signal represents signalling activities of Rho GTPases, which are one of the main regulators of the cytoskeleton (Li et al. 2005). The strength of the activation signal is mathematically given by

$$C = \exp\left(\frac{-t_i}{\theta}\right), \tag{1}$$

where θ is the decay constant of the signal and t_i is the time measured after the onset of an activation signal. This equation is based on the assumption that once an activation signal is received, the strength of the signal suddenly rises to a fully activated state ($C = 1$) and then decays exponentially as the activating molecules start to dissociate from the receptors to which they are bound ($C \rightarrow 0$).

2.1.2 Stress fibre assembly level

The assembly level η represents the degree to which the filamentous actin and phosphorylated myosin are incorporated into a stress fibre, which is fundamental to the contractile performance of a migrating cell. As used here, η is the ratio of the amount of assembly for a stress fibre compared to its maximum possible level ($0 \leq \eta \leq 1$). The rate of assembly level, which depends on the activation signal and the amount of local tension, is represented by

$$\dot{\eta} = \left[(1-\eta)\frac{Ck_f}{\theta}\right] - \left[\left(1-\frac{T}{T_0}\right)\eta\frac{k_b}{\theta}\right], \tag{2}$$

where T is the local tension in the fibre, T_0 is the isometric tension, and k_f and k_b are the forward and backward rate

constants for assembly and disassembly of a stress fibre, respectively. The isometric tension T_0 is defined to be proportional to the assembly level of the stress fibre, $T_0 = \eta T_{max}$, where T_{max} is the maximum isometric tension possible in a stress fibre. Lastly, the over-dot denotes differentiation with respect to time.

As defined in the first term in Equation (2), the rate of stress fibre assembly decreases with current assembly level η due to a limited number of free monomers of actin and unphosphorylated myosin within the cell. With the same reasoning, the second term in Equation (2) describes the rate of stress fibre disassembly and increases with current assembly level η. If Equation (2) was set up as a simple first-order kinetic equation where $\dot{\eta} = (1 - \eta)k_f/\theta - \eta k_b/\theta$, then the assembly level η would increase with increasing time until it reached an equilibrium state that is determined by the values of k_f and k_b (Figure 2, blue line). Likewise, if Equation (2) only incorporated the role of Rho GTPases in stress fibre assembly, then the rate would be given by $\dot{\eta} = C(1 - \eta)k_f/\theta - \eta k_b/\theta$. In this case, the exponential decay in the activation signal would cause the first term to converge to zero, and as such, the disassembly rate would dominate until there was no longer a stress fibre (Figure 2, green line). Finally, incorporating the role of tension into the second term encompasses the findings that tension can promote stress fibre formation (Chaudhuri et al. 2009) and myosin catch bonds (Guo and Guilford 2006), and that compression can inhibit actin polymerisation (Parekh et al. 2005; Prass and Jacobson 2006). The assembly level in Equation (2) is seen to rise and drop because of the decay in the activation signal, but then stabilises at a particular steady-state level. This response is because isometric tension that developed in the stress fibre causes the disassembly term to go to zero, whereas the assembly term also goes to zero because of the activation signal (Figure 2, red line). In this simulation, the forward and backward rate constants were fixed at $k_f = k_b = 5$, and the decay constant was set to $\theta = 1$. The stabilising effect of tension on stress fibre assembly is a simplification of a complex set of different processes (Pellegrin and Mellor 2007). In fact, it is reasonable to consider that high levels of tension can rupture stress fibres, but the intracellular tensions associated with migration are considered here to be far lower than the forces that would cause a cell to pull itself apart.

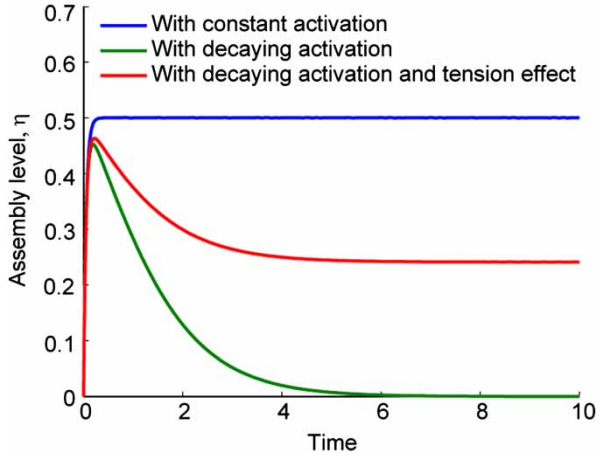

Figure 2. Simulation results of assembly level for three illustrative cases. Forward and backward kinetic rate constants $k_f = k_b = 5$ are used for all simulations.

2.1.3 *Linearised Hill force–velocity relationship*

Stress fibres in non-muscle cells are assumed here to have a similar isotonic relationship as myofibrils in skeletal muscle due to similarities between non-muscle myosin II and muscle myosin II. Hill's model states that contractile tension of tenanised muscle is inversely related to its shortening velocity (McMahon 1984). Here, this hyperbolic relationship is linearised for the relationship between cytoskeletal tension and shortening velocity of a stress fibre,

$$\frac{T}{T_0} = 1 - \frac{k_v v}{\eta v_0}, \tag{3}$$

where v is the rate of change in length of a stress fibre, v_0 is the maximum rate of change and k_v is a velocity constant that relates the reduction in tension due to the shortening velocity (v/v_0). A plot of tension T with respect to the contraction rate v shows that tension decreases as shortening velocity increases (Figure 3). Here, it is noteworthy that the isotonic velocity, which is the shortening velocity at zero tension, is limited by the assembly level and the velocity constant. Since assembly level changes during contractile activity, the isotonic shortening velocity changes in accordance. This is

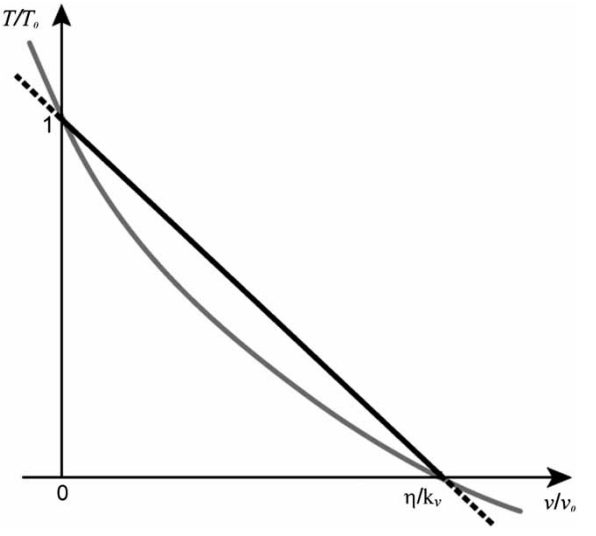

Figure 3. Normalised force–velocity relationship used in the migration model (shown in *black*) is linearised from Hill's muscle model (Hill 1938) (shown in *grey*).

reasonable because if there were no stress fibres assembled ($\eta = 0$), then it would be impossible for a cell to contract, and likewise, there is maximum isotonic velocity when all stress fibres are fully assembled ($\eta = 1$).

2.2 Migration mechanics

On the basis of this contractility model, several key events were incorporated into the time-course of the migration model. First, a relaxed, stationary cell was activated to contract until it reached a steady-state condition. Second, a new adhesion to a post was formed during the extension phase which triggered the reactivation of C, causing whole cell contraction until a new steady state. Lastly, in order to complete the first steps of migration, mechanical release of an adhesion at the rear of a cell was conducted. These settings are designed to illuminate how each step affects cellular contractility in a spatial and temporal fashion.

2.2.1 1D simulation

In this study, we consider a cell lying on an array of posts, in which the spacing between posts and their spring stiffness k_s were equal. The force equilibrium equation about the nth post is given by

$$T_{n+1} - T_n - k_s \Delta x_n = 0, \tag{4}$$

where Δx_n is the deflection of the post, T_n is a tension at the nth stress fibre segment which is defined to be to the left of the nth post and M is the total number of posts underneath a cell. Since there is no stress fibre attached to the left of the first post, by definition the tension in this stress fibre segment is zero ($T_1 = 0$). The relationship between the rate of deflection of the ith post and the rate of change in length of a stress fibre can be written as

$$\dot{x}_i = \dot{x}_{i-1} + v_i. \tag{5}$$

In order to solve Equations (1)–(5), the tension in the nth stress fibre is rewritten from Equation (3) as

$$T_n = T_0\left(1 - \frac{k_v v_n}{\eta_n v_0}\right). \tag{6}$$

By substituting Equation (5) into (6), tension T_n becomes

$$T_n = T_0\left(1 - \frac{k_v}{\eta_n v_0}(\dot{x}_n - \dot{x}_{n-1})\right). \tag{7}$$

Subsequently, substituting this equation into Equation (4) yields the following first-order differential equations that describe the deflection of the posts:

$$\frac{k_v}{v_0} T_{max}\left(\dot{x}_{n+1} - \dot{x}_n\right) + k_s x_n = \eta_{n+1} T_{max}, \quad n = 1, \tag{8a}$$

$$\frac{k_v T_{max}}{v_0}\left(\dot{x}_{n+1} - 2\dot{x}_n + \dot{x}_{n-1}\right) + k_s x_n = \left(\eta_{n+1} - \eta_n\right) T_{max}, \quad 1 < n < M, \tag{8b}$$

$$\frac{k_v T_{max}}{v_0}(-\dot{x}_n + \dot{x}_{n-1}) + k_s x_n = -\eta_n T_{max}, \quad n = M. \tag{8c}$$

This set of equations leads to a matrix form of equations expressed as

$$\mathbf{A}\dot{\mathbf{x}} + k_s \mathbf{I}\mathbf{x} = \mathbf{T}, \tag{9}$$

where $\mathbf{I}$ is the identity matrix and,

$$\mathbf{A} = \begin{bmatrix} -\frac{k_v T_{max}}{v_0} & \frac{k_v T_{max}}{v_0} & 0 & 0 & 0 \\ \frac{k_v T_{max}}{v_0} & -\frac{2k_v T_{max}}{v_0} & \frac{k_v T_{max}}{v_0} & 0 & 0 \\ 0 & \ddots & \ddots & \ddots & 0 \\ 0 & 0 & \frac{k_v T_{max}}{v_0} & -\frac{2k_v T_{max}}{v_0} & \frac{k_v T_{max}}{v_0} \\ 0 & 0 & 0 & \frac{k_v T_{max}}{v_0} & -\frac{k_v T_{max}}{v_0} \end{bmatrix},$$

$$\mathbf{T} = \begin{bmatrix} \eta_2 T_{max} \\ (\eta_3 - \eta_2) T_{max} \\ \vdots \\ (\eta_{n+1} - \eta_n) T_{max} \\ \vdots \\ (\eta_M - \eta_{M-1}) T_{max} \\ -\eta_M T_{max} \end{bmatrix}, \quad \dot{\mathbf{x}} = \begin{bmatrix} \dot{x}_1 \\ \dot{x}_2 \\ \vdots \\ \dot{x}_n \\ \vdots \\ \dot{x}_{M-1} \\ \dot{x}_M \end{bmatrix} \quad \text{and}$$

$$\mathbf{x} = \begin{bmatrix} x_1 \\ x_2 \\ \vdots \\ x_n \\ \vdots \\ x_{M-1} \\ x_M \end{bmatrix}.$$

In the matrix form of equations, $\mathbf{A}$ is singular and so the deflections $\mathbf{x}$ are solved for using Matlab function ode15, which is specialised in solving differential algebraic equations.

For assembly level, Equation (2) was used to determine the level of assembly in each stress fibre segment.

Table 1. Model parameters for 1D simulation.

Parameters	Description	Values
k_s	Spring constant of a post	3
k_v	Force reduction coefficient with respect to strain rate	1.5
$\dot{v}_0$	Maximum extension rate of a stress fibre	0.4
T_{max}	Maximum stress of a cell	1
k_f	Assembly rate constant	3
k_b	Disassembly rate constant	2
θ	Time decay constant	1

To express this in indicial notation, the equation for the assembly level can be written as

$$\dot{\eta}_i = \left[(1-\eta_i)\frac{Ck_f}{\theta}\right] - \left[\left(1-\frac{T_i}{T_0}\right)\eta_i\frac{k_b}{\theta}\right], \quad 1 \le i \le M. \tag{10}$$

These equations were solved with explicit Euler's method with initial conditions of $\eta_i = T_i = x_i = 0$ at $t = 0$. Steady state during the initial contraction phase was defined as the time after which the change in post deflections reached zero. Once at steady state, the extension phase was begun where the number of total posts was increased by one. Simultaneously, a new activation signal C was begun in the whole cell. Once a new steady state was reached, the rear adhesion to post 1 was removed by setting the tension in the stress fibre T_2 to zero. The simulation was run until a new steady state in contractility was reached. Model parameters regarding 1D simulation are listed in Table 1.

2.2.2 2D simulation

A 2D computational model of the migrating cell was constructed using the finite element method. In the model, a cell was assumed as an isotropic, continuous material in which the stress fibre formation at any nodal point depends on the stresses at the position. As before as in the 1D simulation, Equation (1) is used to describe the activation signal. However, the assembly level in 2D was generalised as

$$\dot{\eta} = \left[(1-\eta)\frac{Ck_f}{\theta}\right] - \left[\left(1-\frac{\sigma_I}{\sigma_0}\right)\eta\frac{k_b}{\theta}\right], \tag{11}$$

where σ_0 is the isometric stress, $\sigma_0 = \eta\sigma_{max}$. The stress σ_{max} is the maximum that a stress fibre can bear. Here, σ_I is the average first stress invariant, $\sigma_I = (\sigma_{x,active} + \sigma_{y,active})/2$, where $\sigma_{x,active}$ and $\sigma_{y,active}$ are the active normal stresses in the x- and y-direction, respectively. The first stress invariant was chosen as a parameter representing the tensional state at a certain node because it depicts the level of total stress in a cell and is independent of orientation or coordinate system. In 2D simulations, the constitutive equation for stresses σ_x and σ_y incorporates components of passive elasticity from the cytoskeleton and cytoplasmic structures and components of active stress derived from the Hill-like force–velocity relationship

$$\sigma_i = \sigma_{i,active} + \sigma_{i,passive}, \tag{12}$$

where

$$\sigma_{i,active} = \eta\sigma_{max}\left(1 + \frac{k_v\dot{\varepsilon}_i}{\eta\dot{\varepsilon}_0}\right), \tag{13}$$

$$\sigma_{i,passive} = E\frac{(1-\nu)\varepsilon_i + \nu(\varepsilon_j + \varepsilon_k)}{(1+\nu)(1-2\nu)}. \tag{14}$$

Here, i is either the x- or y-direction where a state of plane stress is assumed, $\dot{\varepsilon}_i$ is the strain rate in the ith direction, $\dot{\varepsilon}_0$ is the maximum strain rate that a stress fibre can bear, σ_0 is the isometric stress in a stress fibre, ν is Poisson's ratio of a cell, E is its elastic modulus and j and k are the other two Cartesian directions. A linear isotropic stress–strain relationship is assumed for the passive elasticity of the cell. The structural analysis for stress–strain evaluation was combined with a weak-form-based partial differential equation (PDE) solver for the stress fibre assembly level as a module in Comsol Multiphysics 3.5a (Comsol, Inc., Burlington, MA). A cell supported between four bracket-shaped posts was chosen for its simplified dimensional constraints.

To simulate cell migration, the model was solved transiently for each step of the process – contraction, extension and release – and the simulation did not progress into the next stage until the stress in the cell reached steady state. To start the contraction phase, the cell was bound to three posts at its corners (Figure 6, left). The steady-state values for assembly level, deformation, stresses and strains were used as initial conditions for the following extension phase. At the start of the extension phase, a new adhesion to a fourth post was created and a new activation signal C was applied to the entire cell (Figure 6, middle). As before, the steady-state values were subsequently used as the initial condition for the simulation during the release phase. Here, the post at the trailing edge (upper-right) was removed, and the simulation was run to find a new contractile state (Figure 6, right). Quadratic Lagrange elements in Comsol were used in the simulation. The side length of the square-shaped cell was drawn to 9 μm, whereas the thickness was set to be 1 μm. The model parameters used in 2D simulation are listed in Table 2. In the simulation, the cell begins to contract from completely unassembled state, i.e. $\eta = 0$ at $t = 0$.

3. Results

As was previously discussed in the model's description, a cell was simulated to undergo a contraction, extension and release phase over the course of the simulations on posts (Figure 4, Top). The first steps in migration of a cell on 1D

Table 2. Model parameters for 2D simulation.

Parameters	Description	Values	References
E_{cell}	Young's modulus of a cell	250 Pa	Guilak et al. (2000)
v_{cell}	Poisson's ratio of a cell	0.36	Trickey et al. (2006)
E_{sub}	Young's modulus of a substrate	1000 Pa	–
v_{sub}	Poisson's ratio of a substrate	0.49	–
k_v	Force reduction coefficient with respect to strain rate	1.5	Same as 1D
$\dot{\varepsilon}_0$	Maximum extension rate of a stress fibre	0.2 s^{-1}	Deshpande et al. (2007)
σ_{max}	Maximum stress of a cell	25 Pa	–
k_f	Assembly rate constant	5	–
k_b	Disassembly rate constant	3	–
θ	Time decay constant	1 s	Same as 1D

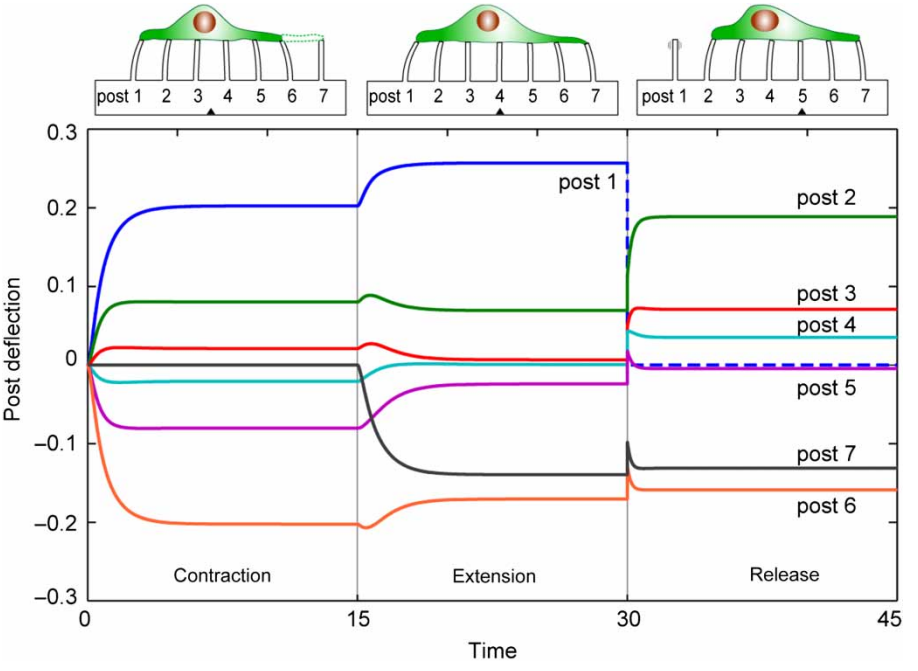

Figure 4. 1D simulation of cell migration on an array of posts. (Top) Schematic illustration depicts a cell during each phase of migration. The deflection of the posts by the cell's traction forces has been added as a visual aid and are not drawn to scale. The black arrowheads denote the point of force equilibrium, where the sums of the forces on either side of the cell are equal. (Bottom) Results of post deflections from the 1D simulation show that there are spatial and temporal changes in traction forces in each phase of migration.

posts are predicted to cause post deflections that are spatially and temporally different from each other (Figure 4). In the contraction phase, post deflections increased until they reached a steady state where the activation signal decayed to a negligible level and tension developed in the stress fibres kept the assembly level from returning to zero. Spatially during the contraction phase, the largest deflections were observed at the edge posts (posts 1 and 6). Contrarily, the inner posts experienced smaller deflections because tensions in the stress fibres attached to the post were mostly counterbalancing with each other and left only small resultant forces to be supported by the posts. The result at the initial contraction phase shows the validity in our model because similar patterns of post deflections were observed in previous efforts of the bio-chemical–mechanical model (Deshpande et al. 2007).

At the beginning of the extension phase, the new post (post 7 in Figure 4) started to deflect towards a cell centre. The previous edge post (post 6) also deflected inward due to the influence of the new activation signal. But shortly thereafter, the deflection of post 6 decreased along with the remaining inner posts (post 2 to post 5) in order to counterbalance the new deflection at post 7. Interestingly enough, the post on the trailing edge (post 1) deflected more noticeably in the centripetal direction, which resulted in its force being largest among all posts. This finding agrees with direct measurements of traction forces, where the highest forces were observed at the tail region of a migrating cell (Galbraith and Sheetz 1997).

When the adhesion to the post at the tail was released, a sudden rearrangement of forces occurred to satisfy force equilibrium. Post 2, which had previously been adjacent to the tail, deflected further inward due to the loss of counterbalancing force from the released stress fibre. Likewise, the rest of posts also deflected towards the leading edge in a transient fashion as the stress fibres within the cell adjusted to the new levels of tensions. The resulting steady-state deflections were no longer symmetric about the geometric centre of the cell as had been previously seen in the contraction phase.

During the migration process, the force equilibrium point was identified to denote the forward progression of the cell. The point of force equilibrium is where the sum of the magnitudes of forces on either side of the cell is equal. In the contraction phase, the equilibrium point laid between posts 3 and 4, which coincided with the geometric centre of the cell, because there was a lack of polarisation within the cell. Subsequently, the equilibrium point advanced to post 4 in the extension phase and also coincided with the new geometric centre of the cell. During release, the equilibrium point resided at post 5, which was not the geometric centre and signified that the cell had reached a polarised state. The steady advancement of the equilibrium point implicates that the contractility model is capable of predicting the translocation of the cell body as well as the onset of a polarised contractile cytoskeleton.

To quantify the contractility of the whole cell over time, the strain energy stored in the posts was calculated (Figure 5, solid line). As expected, the strain energy rose rapidly during the contraction phase until it reached a steady state. The strain energy increased again following the second activation signal during the extension phase.

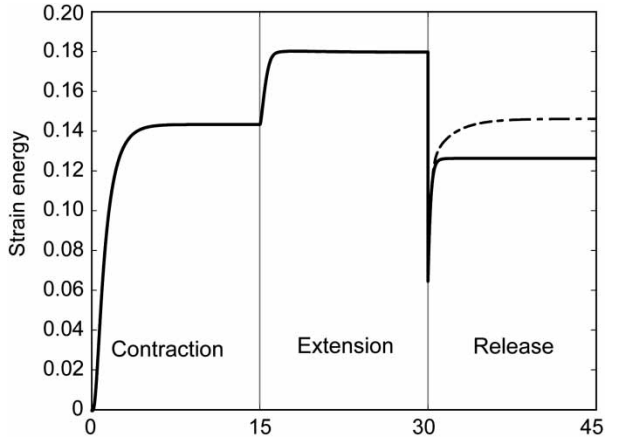

Figure 5. Strain energy in the posts by a cell's contraction in the 1D simulation. Strain energy increases during the extension phase, but drops during the release phase to a level below steady-state contraction (solid line). If another activation signal is initiated at the start of the release phase (dotted line), then strain energy can be restored to levels that are close to steady-state contraction.

Interestingly, contractility dropped upon adhesion release to a level that was lower than the steady state during the contraction phase. This response during the release phase was due to the sudden loss in tension at post 1 which subsequently caused disassembly of stress fibres until a new assembly level and corresponding tensional state were reached. What is surprising is that the model indicates that a large amount of energy is lost during a migration cycle. Furthermore, simulating multiple migration cycles can cause the overall contractility to significantly decrease. Indeed, previous experimental studies have reported that adhesion detachment in a cell causes a remarkable loss of tension (Burton et al. 1999; Roy et al. 1999), strain energy (Del Alamo et al. 2007) and phosphorylated myosin light chain (Ren et al. 2004). This result necessitated us to hypothesise a means for a cell to recover its state of contractility to a steady level. We speculated that another activation signal may occur upon release to compensate the loss of contractility. Performing a new simulation of a complete migration cycle with this third activation signal revealed that a cell can recover its loss in strain energy in order to maintain a constant degree of contractility during migration (Figure 5, dashed line).

To check and compare the 1D simulation to what is observed *in vitro*, we constructed a 2D simulation of migration (Figure 6). A spatial plot of the assembly level during the contraction phase showed a high concentration of stress fibres in the vicinity of the adhesions to the three supporting posts, which is in agreement with a previous model of cells contracting on posts in 2D (Figure 7(A)) (Deshpande et al. 2006). These focal-like concentrations of stress fibres are also shown in the extension and release phases, although their degrees of magnitude are different. In the extension phase, all four of the adhesions have highly concentrated stress fibres, whereas the adhesions lose their stress fibre assembly levels upon the release of an adhesion.

To quantify the overall contractility of the cell, the strain energy of the posts was obtained by integrating the strain energy density over the area of each support (Figure 7(B)). The contractility showed a remarkably similar behaviour as observed in the simulation of 1D cell migration. Contractility was shown to increase upon new adhesion formation, but dropped upon release (black line). After release, an oscillation in strain energy occurs which quickly dampens and reaches steady state (dotted line). It is noteworthy that the steady-state level after the release is, again, below the steady-state level in the contraction phase. As before, we applied a third activation signal at the time of release and found it was essential to maintaining cytoskeletal tension during migration (grey line). Therefore, the results from both our 1D and 2D migration simulations strongly suggest that cells use biochemical activation to supplement the loss in cytoskeletal tension upon adhesion release.

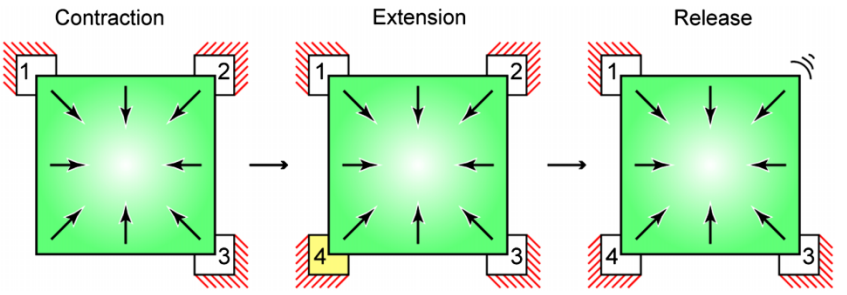

Figure 6. Schematic illustration of cell migration for 2D simulations performed in Comsol. Initially, the cell contracts against posts 1–3 and then migrates by extending towards post 4 and releasing from post 2.

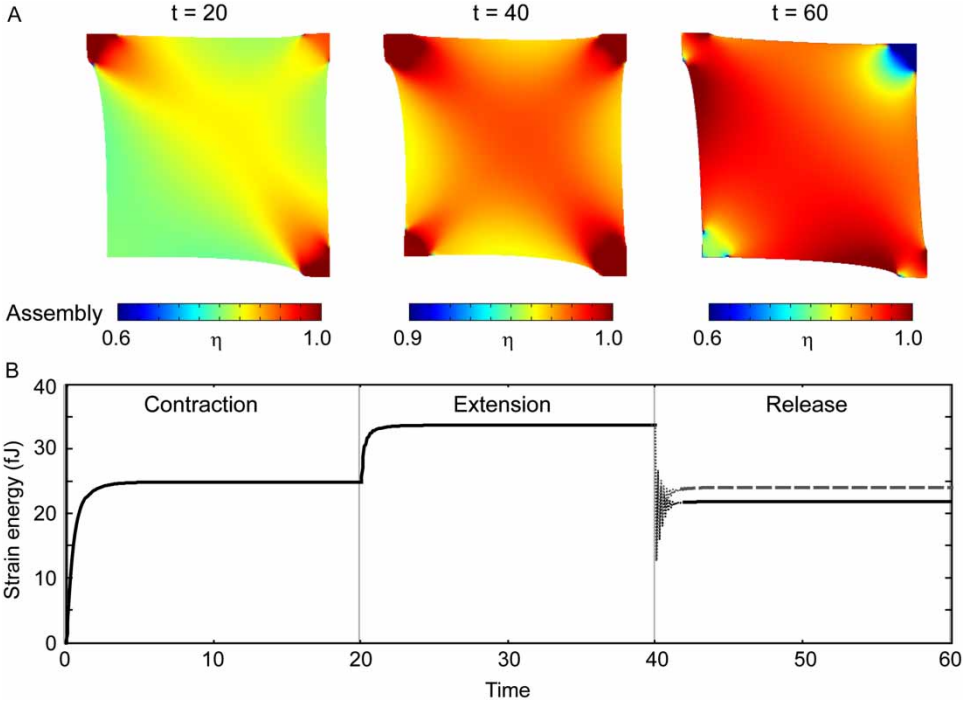

Figure 7. Simulation results from the 2D migration model. (A) Spatial map depicting the assembly level at the end of each phase of migration. (B) Strain energy in the posts increases during the contraction phase, increases further in the extension phase and drops significantly during the release phase (black line). If an activation signal is added at the start of the release phase (grey line), contractility is restored to levels similar to those in the contraction phase.

4. Discussion

We have described a computational model to address how cellular contractility is coordinated as a cell migrates across an array of posts. The model simulated the traction forces generated during one complete cycle of migration by incorporating activation signals that occurred during initial contraction and new adhesion formation, kinetic models of stress fibre assembly and biomechanical relationships between traction stress and shortening velocity. Thus, this approach is fundamentally different from the diffusion-based models or the lumped parameter models for cell migration because it allowed for a close comparison between the results of the model and the measurements of traction forces seen with post arrays and deformable substrates. Although the simulations focused on cell migration on post arrays, the framework of the model can be applied to analyzing the contractile process of cell migration in a variety of cell assays or environments.

A cell migrating on a 1D post array had several spatiotemporal features commonly seen in cell migration: large forces at the trailing and leading edge and the forward progression of the cell body. Interestingly, the large forces at the two edges of the cell were predicted solely by the condition of force equilibrium. This feature was in agreement with the finding that the tail of a cell and the leading edge have the largest forces (Galbraith and Sheetz 1997; Munevar et al. 2001). Several studies have shown that cell retraction is closely related to increased levels of

phosphorylated myosin that coordinates with tyrosine phosphorylation and calpain activity to release the adhesions at the rear (Crowley and Horwitz 1995; Palecek et al. 1998; Zeng et al. 2000; Huang et al. 2008; Sen et al. 2009; Wildt et al. 2009). Together with weakened adhesion strength, the high force at the tail during the extension phase can contribute to rear detachment by overcoming the adhesion strength of focal adhesion (Parsons et al. 2010).

Quantification of strain energy in both 1D and 2D simulations showed that there was a drop in cell contractility upon release. A loss of contractility was observed in migration studies where tail retractions led to a dramatic reduction in deformation of the substrate (Burton et al. 1999; Roy et al. 1999). Moreover, strain energy exerted by migrating cells was seen to have cyclic nature, where strain energy in a substrate increases upon a new adhesion formation and decreases upon adhesion release (Del Alamo et al. 2007). In addition, cell detachment with trypsin can significantly reduce the amount of phosphorylated myosin, although the result was obtained from whole cell detachment (Ren et al. 2004). Taken together, it is likely that new adhesions cause an increase in contractility and tail retraction causes a loss, but it is uncertain whether contractility falls below steady-state levels seen in stationary cells.

Ultimately, our simulations raise an important question: How can a cell maintain its contractility after it takes its first step? When another activation signal was added to the release phase in both models, overall cell contractility could be maintained at levels similar to those in stationary cells. A study that performed a simultaneous visualisation of Rho GTPase activity showed that Cdc42 and Rac1maintain a high activity level during the release phase and continue until the next protrusion cycle (Machacek et al. 2009). Considering that Cdc42, like RhoA, can affect cytoskeletal contractility via myotonic dystrophy kinase-related Cdc42-binding kinase which phosphorylates myosin to regulate cell retraction (Groeger and Nobes 2007), our simulations suggest that a cell might regulate another signalling pathway to maintain its tensional homeostasis during migration.

The bio-chemical–mechanical model for migration can be used to examine a wider range of mechanical factors that affect cell migration such as durotaxis, haptotaxis and topotaxis (Harris 1973; Lo et al. 2000; Kim et al. 2009). The model can also include the cytoskeletal aspects that regulate adhesion maturation because they are driven by the balance of actin polymerisation and actin–myosin contraction (Parsons et al. 2010). Eventually, these efforts will need to incorporate the nature of cytoskeletal protrusions in order to adequately simulate a cell's advancement to a new adhesion spot and thereby provide important motility properties such as velocity and orientation in addition to the traction forces predicted thus far.

Acknowledgements

We thank Peizhe Shi, Lucas Ting, Shirin Fegghi, Marita Rodriguez and Wes Tooley for helpful discussions. This work is funded by an NSF CAREER Award.

References

Bray D. 2001. Cell movements: from molecules to motility. New York: Garland Publishers.

Burton K, Park JH, Taylor DL. 1999. Keratocytes generate traction forces in two phases. Mol Biol Cell. 10:3745–3769.

Carter SB. 1967. Haptotaxis and the mechanism of cell motility. Nature. 213(5073):256–260.

Chaplain MA. 2000. Mathematical modelling of angiogenesis. J Neurooncol. 50(1–2):37–51.

Chaudhuri O, Parekh SH, et al. 2009. Combined atomic force microscopy and side-view optical imaging for mechanical studies of cells. Nat Methods. 6(5):383–387.

Chicurel M. 2002. Cell biology. Cell migration research is on the move. Science. 295(5555):606–609.

Crowley E, Horwitz AF. 1995. Tyrosine phosphorylation and cytoskeletal tension regulate the release of fibroblast adhesions. J Cell Biol. 131(2):525–537.

Del Alamo JC, Meili R, Alonso-Latorre B, Rodriguez-Rodriguez J, Aliseda A, Firtel RA, Lasheras JC. 2007. Spatio-temporal analysis of eukaryotic cell motility by improved force cytometry. Proc Natl Acad Sci USA. 104:13343–13348.

Dembo M, Wang YL. 1999. Stresses at the cell-to-substrate interface during locomotion of fibroblasts. Biophys J. 76(4): 2307–2316.

Deshpande VS, McMeeking RM, Evans AG. 2006. A bio-chemo-mechanical model for cell contractility. Proc Natl Acad Sci USA. 103:14015–14020.

Deshpande VS, McMeeking RM, Evans AG. 2007. A model for the contractility of the cytoskeleton including the effects of stress-fibre formation and dissociation. Proc Royal Soc Math Phys Eng Sci. 463:787–815.

Devreotes PN, Zigmond SH. 1988. Chemotaxis in eukaryotic cells: a focus on leukocytes and Dictyostelium. Annu Rev Cell Biol. 4:649–686.

DiMilla PA, Barbee K, Lauffenburger DA. 1991. Mathematical model for the effects of adhesion and mechanics on cell migration speed. Biophys J. 60:15–37.

Dokukina IV, Gracheva ME. 2010. A model of fibroblast motility on substrates with different rigidities. Biophys J. 98(12): 2794–2803.

du Roure O, Saez A, Buguin A, Austin RH, Chavrier P, Silberzan P, Ladoux B. 2005. Force mapping in epithelial cell migration. Proc Natl Acad Sci USA. 102:2390–2395.

Galbraith CG, Sheetz MP. 1997. A micromachined device provides a new bend on fibroblast traction forces. Proc Natl Acad Sci USA. 94(17):9114–9118.

Gerisch A, Chaplain MA. 2008. Mathematical modelling of cancer cell invasion of tissue: local and non-local models and the effect of adhesion. J Theor Biol. 250(4):684–704.

Ghibaudo M, Saez A, Trichet L, Xayaphoummine A, Browaeys J, Silberzan P, Buguin A, Ladoux B. 2008. Traction forces and rigidity sensing regulate cell functions. Soft Matter. 4: 1836–1843.

Giannone G, Sheetz MP. 2006. Substrate rigidity and force define form through tyrosine phosphatase and kinase pathways. Trends Cell Biol. 16(4):213–223.

Gracheva ME, Othmer HG. 2004. A continuum model of motility in ameboid cells. Bull Math Biol. 66(1):167–193.

Groeger G, Nobes CD. 2007. Co-operative Cdc42 and Rho signalling mediates ephrinB-triggered endothelial cell retraction. Biochem J. 404(1):23–29.

Guilak F, Tedrow JR, Burgkart R. 2000. Viscoelastic properties of the cell nucleus. Biochem Biophys Res Commun. 269: 781–786.

Guo B, Guilford WH. 2006. Mechanics of actomyosin bonds in different nucleotide states are tuned to muscle contraction. Proc Natl Acad Sci USA. 103(26):9844–9849.

Harris A. 1973. Behavior of cultured cells on substrata of variable adhesiveness. Exp Cell Res. 77(1):285–297.

Harris AK, Wild P, Stopak D. 1980. Silicone rubber substrata: a new wrinkle in the study of cell locomotion. Science. 208: 177–179.

Hill AV. 1938. The heat of shortening and the dynamic constants of muscle. Proc Royal Soc London Ser B Biol Sci. 126(843): 136–195.

Huang X, Wu D, Jin H, Stupack D, Wang JY. 2008. Induction of cell retraction by the combined actions of Abl–CrkII and Rho-ROCK1 signaling. J Cell Biol. 183:711–723.

Kim DH, Seo CH, Han K, Kwon KW, Levchenko A, Suh KY. 2009. Guided cell migration on microtextured substrates with variable local density and anisotropy. Adv Funct Mater. 19:1579–1586.

Kirfel G, Rigort A, Borm B, Herzog V. 2004. Cell migration: mechanisms of rear detachment and the formation of migration tracks. Eur J Cell Biol. 83:717–724.

Lauffenburger DA, Horwitz AF. 1996. Cell migration: a physically integrated molecular process. Cell. 84(3): 359–369.

Lemmon CA, Sniadecki NJ, Ruiz SA, Tan JL, Romer LH, Chen CS. 2005. Shear force at the cell-matrix interface: enhanced analysis for microfabricated post array detectors. Mech Chem Biosyst. 2:1–16.

Li S, Butler P, Wang Y, Hu Y, Han DC, Usami S, Guan JL, Chien S. 2002. The role of the dynamics of focal adhesion kinase in the mechanotaxis of endothelial cells. Proc Natl Acad Sci USA. 99:3546–3551.

Li S, Guan JL, Chien S. 2005. Biochemistry and biomechanics of cell motility. Annu Rev Biomed Eng. 7:105–150.

Liang XM, Han SJ, Reems JA, Gao D, Sniadecki NJ. 2010. Platelet retraction force measurements using flexible post force sensors. Lab Chip. 10:991–998.

Liu Z, Tan JL, Cohen DM, Yang MT, Sniadecki NJ, Ruiz SA, Nelson CM, Chen CS. 2010. Mechanical tugging force regulates the size of cell–cell junctions. Proc Natl Acad Sci USA. 107:9944–9949.

Lo CM, Wang HB, Dembo M, Wang YL. 2000. Cell movement is guided by the rigidity of the substrate. Biophys J. 79: 144–152.

Machacek M, Hodgson L, Welch C, Elliott H, Pertz O, Nalbant P, Abell A, Johnson GL, Hahn KM, Danuser G. 2009. Coordination of Rho GTPase activities during cell protrusion. Nature. 461:99–103.

Maree AF, Jilkine A, Dawes A, Grieneisen VA, Edelstein-Keshet L. 2006. Polarization and movement of keratocytes: a multiscale modelling approach. Bull Math Biol. 68: 1169–1211.

McGarry JP, Fu J, Yang MT, Chen CS, McMeeking RM, Evans AG, Deshpande VS. 2009. Simulation of the contractile response of cells on an array of micro-posts. Philos Trans A Math Phys Eng Sci. 367:3477–3497.

McMahon TA. 1984. Muscles, reflexes, and locomotion. Princeton, NJ: Princeton University Press.

Mitrossilis D, Fouchard J, Guiroy A, Desprat N, Rodriguez N, Fabry B, Asnacios A. 2009. Single-cell response to stiffness exhibits muscle-like behavior. Proc Natl Acad Sci USA. 106: 18243–18248.

Munevar S, Wang Y, Dembo M. 2001. Traction force microscopy of migrating normal and H-ras transformed 3T3 fibroblasts. Biophys J. 80:1744–1757.

Palecek SP, Huttenlocher A, Horwitz AF, Lauffenburger DA. 1998. Physical and biochemical regulation of integrin release during rear detachment of migrating cells. J Cell Sci. 111(Pt 7):929–940.

Parekh SH, Chaudhuri O, Theriot JA, Fletcher DA. 2005. Loading history determines the velocity of actin-network growth. Nat Cell Biol. 7:1219–1223.

Parsons JT, Horwitz AR, Schwartz MA. 2010. Cell adhesion: integrating cytoskeletal dynamics and cellular tension. Nat Rev Mol Cell Biol. 11:633–643.

Pellegrin S, Mellor H. 2007. Actin stress fibres. J Cell Sci. 120(Pt 20):3491–3499.

Prass M, Jacobson K, Mogilner A, Radmacher M. 2006. Direct measurement of the lamellipodial protrusive force in a migrating cell. J Cell Biol. 174:762–772.

Ren XD, Wang R, Li Q, Kahek LA, Kaibuchi K, Clark RA. 2004. Disruption of Rho signal transduction upon cell detachment. J Cell Sci. 117:3511–3518.

Rigort A, Grunewald J, Herzog V, Kirfel G. 2004. Release of integrin macroaggregates as a mechanism of rear detachment during keratinocyte migration. Eur J Cell Biol. 83:725–733.

Roy P, Petroll WM, Chuong CJ, Cavanagh HD, Jester JV. 1999. Effect of cell migration on the maintenance of tension on a collagen matrix. Ann Biomed Eng. 27:721–730.

Saez A, Buguin A, Silberzan P, Ladoux B. 2005. Is the mechanical activity of epithelial cells controlled by deformations or forces? Biophys J. 89:L52–L54.

Sen S, Engler AJ, Discher DE. 2009. Matrix strains induced by cells: Computing how far cells can feel. Cell Mol Bioeng. 2: 39–48.

Sheetz MP, Felsenfeld D, Galbraith CG, Choquet D. 1999. Cell migration as a five-step cycle. Biochem Soc Symp. 65: 233–243.

Tan JL, Tien J, Pirone DM, Gray DS, Bhadriraju K, Chen CS. 2003. Cells lying on a bed of microneedles: an approach to isolate mechanical force. Proc Natl Acad Sci USA. 100(4): 1484–1489.

Thackham JA, McElwain DL, Turner IW. 2009. Computational approaches to solving equations arising from wound healing. Bull Math Biol. 71:211–246.

Trickey WR, Baaijens FP, Laursen TA, Alexopoulos LG, Guilak F. 2006. Determination of the Poisson's ratio of the cell: recovery properties of chondrocytes after release from complete micropipette aspiration. J Biomech. 39(1):78–87.

Tranquillo RT, Lauffenburger DA, Zigmond SH. 1988. A stochastic model for leukocyte random motility and chemotaxis based on receptor binding fluctuations. J Cell Biol. 106:303–309.

Wildt B, Wirtz D, Searson PC. 2009. Programmed subcellular release for studying the dynamics of cell detachment. Nat Methods. 6:211–213.

Zeng Q, Lagunoff D, Masaracchia R, Goeckeler Z, Cote G, Wysolmerski R. 2000. Endothelial cell retraction is induced by PAK2 monophosphorylation of myosin II. J Cell Sci. 113(Pt 3):471–482.